ON SYNCHRONIZATION OF WIRELESS ACOUSTIC SENSOR NETWORKS IN THE PRESENCE OF TIME-VARYING SAMPLING RATE OFFSETS AND SPEAKER CHANGES

Tobias Gburrek, Joerg Schmalenstroeer, Reinhold Haeb-Umbach

Department of Communications Engineering, Paderborn University, Germany
{gburrek, schmalen, haeb}@nt.uni-paderborn.de

ABSTRACT

A wireless acoustic sensor network records audio signals with sampling time and sampling rate offsets between the audio streams, if the analog-digital converters (ADCs) of the network devices are not synchronized. Here, we introduce a new sampling rate offset model to simulate time-varying sampling frequencies caused, for example, by temperature changes of ADC crystal oscillators, and propose an estimation algorithm to handle this dynamic aspect in combination with changing acoustic source positions. Furthermore, we show how estimates of the distances between microphones and human speakers can be used to determine the sampling time offsets. This enables a synchronization of the audio streams to reflect the physical time differences of flight.

Index Terms— Synchronization, time-varying sampling rate offset, sampling time offset

1. INTRODUCTION

Sampling rate offset (SRO) and sampling time offset (STO) estimation have received a lot of interest in recent years [1–6]. In particular, in the context of wireless acoustic sensor networks (WASNs) these topics are important, because for many signal processing tasks, such as acoustic beamforming [7], the audio signals must be synchronized.

SROs are caused by the differences in the actual frequencies of the oscillators driving the analog-digital converters (ADCs) of the distributed devices despite their equal nominal frequencies [8]. The author of [9] showed that typical SRO values range between -500 parts per million(ppm) and 400 ppm from the nominal frequency for handheld devices, such as smartphones. STOs arise due to the fact that the devices start recording at different moments in time.

The vast majority of works on SRO and STO estimation from the recorded audio signals are conducted under the assumptions of constant SROs and fixed positions of sources and sensors, which, however, are unrealistic for many practical scenarios. The frequency of a crystal oscillator is not only determined by the crystal's shape and the technique utilized to cut it, but is also influenced by a variety of environmental factors, such as aging, temperature, humidity and supply voltage [10]. While constant or slowly changing factors, like aging, are sufficiently accurately modeled by assuming a constant SRO, temperature and supply voltage can change more rapidly and challenge the assumption of constant SROs [8]. In [11] the authors noted that when the device is switched on or when it transits from sleeping to processing mode, the change of the device's temperature incurs a sampling rate change of several ppm within a relatively short period of time (a few minutes). But even after warm-up the SRO can be time-varying, e.g., due to fluctuations of the supply voltage, which are caused by the changing workload of the microprocessor [8]. This all stands in conflict with the assumption of constant SROs

for relatively long time intervals of, e.g., several minutes, made by several SRO estimation algorithms.

Likewise, the assumption of a fixed position of the acoustic source, that is made by most synchronization algorithms that estimate the SRO from the acoustic signals received by the devices, is not given in many application scenarios of a WASN. Consider, for example, a meeting where different participants, each speaking at a different position relative to the sensor network. Handling moving speakers would be even more complicated. Estimating an SRO from signals emitted by a moving source faces the challenging task of separating the SRO-induced delays from delays caused by source position changes. A reasonable simplification is to focus on time periods where the positions remain fixed and to skip transient phases, as proposed in [5].

In this contribution we attempt to overcome some of the above mentioned assumptions. First, we will model the time-varying SROs with an Ornstein-Uhlenbeck process [12] and devise an algorithm for SRO estimation. We discuss the necessary modifications to a previously proposed coherence drift based online algorithm [6] to deal with source position changes and time-varying SROs. Second, we consider STO estimation by separating time delay estimates into the contribution of the recording start times and the contribution from the time differences of flight (TDOFs) from the speakers' positions to the sensors. The latter requires an estimate of the distance of the speaker to the microphones, which is obtained from a deep neural network (DNN) based distance estimator [13]. By discriminating these different contributions we arrive at an STO estimate that regards the physical TDOFs. This is important, e.g., if the location of the sensor nodes is to be estimated from time-difference of arrival (TDOA) estimates.

The paper is organized as follows: In Sec. 2 we discuss the impact of time-varying SROs on signals and show in Sec. 3 our modifications to handle dynamic scenarios with source position changes and time-varying SROs during SRO estimation. Subsequently, STO estimation is presented in Sec. 4. Our approach for modeling time-varying SROs is explained in Sec. 5, before we discuss the experiments in Sec. 6 and end with the conclusions drawn in Sec. 7.

2. PROBLEM STATEMENT

We consider a WASN consisting of two sensor nodes and an unknown SRO and STO between them. Each sensor node is equipped with at least two microphones whose signals are synchronously sampled. Furthermore, we assume that both sensor nodes record the signals emitted by sources at M stationary positions whereby at most one source is active at any given time. Additionally, we consider that there might be short periods of time without source activity when the source position changes. Such a scenario could be typical of a

meeting with multiple participants sitting around a conference table with multiple microphone arrays in the middle.

To simplify the presentation, only the first microphone channel of each sensor node will be reflected in the notation. The continuous-time microphone signal of the i-th sensor node, with $i \in \{1, 2\}$, is given by

$$y_i(t) = \sum_{m=1}^{M} h_i^{(m)}(t) * x^{(m)}(t) + v_i(t), \qquad (1)$$

with $x^{(m)}(t)$ being the source signal emitted at the m-th position and $v_i(t)$ representing white Gaussian sensor noise. $h_i^{(m)}(t)$ denotes the room impulse response (RIR) modeling the sound propagation from the m-th source position to the position of the i-th microphone.

Typically, the sampling processes of the microphone signals will start at different points in time resulting in the STO T_i. In addition to that, the sampling frequency of the i-th microphone $f_i[n] = (1 + \varepsilon_i[n]) \cdot f_s$ will slightly deviate from the nominal sampling frequency f_s. Here, n denotes the discrete-time sample index and $\varepsilon_i[n]$ the time-varying SRO of the i-th microphone with $|\varepsilon_i[n]| \ll 1$. Sampling the i-th microphone signal results in the following discrete-time signal (with $1/(1 + x) \approx 1 - x$ if $|x| \ll 1$):

$$y_i[n] = y_i \left(T_i + \sum_{\tilde{n}=0}^{n-1} \frac{1}{f_s \cdot (1 + \varepsilon_i[\tilde{n}])} \right)$$

$$\approx y_i \left(\frac{n}{f_s} - \frac{1}{f_s} \cdot \underbrace{\left(-T_i \cdot f_s + \sum_{\tilde{n}=0}^{n-1} \varepsilon_i[\tilde{n}] \right)}_{:= \tau_i[n]} \right). \qquad (2)$$

Compared to the synchronous signal $y_i^{(\text{sync})}[n]$ being sampled with the nominal sampling frequency f_s ($\varepsilon_i[n] = 0$ ppm and $T_i = 0$ s) $y_i[n]$ shows a shift of $\tau_i[n]$ samples.

Usually, the microphone signals are processed in a frame-oriented fashion, e.g., in the short-time Fourier transform (STFT) domain. If the shift $\tau_i[n]$ is much smaller than the STFT frame size N the relation between the asynchronously sampled signal $y_i[n]$ and the synchronously sampled signal $y_i^{(\text{sync})}[n]$ can be modeled in the STFT-domain as follows [3, 4, 14]:

$$Y_i(lB, k) \approx Y_i^{(\text{sync})}(lB, k) \cdot \exp \left(-j \frac{2\pi k}{N} \bar{\tau}_i[l] \right), \qquad (3)$$

with frame index l, frequency bin index k and frame shift B. In addition, the SRO is assumed to change slowly and is therefore approximated by $\bar{\varepsilon}_i[l]$ during a STFT frame. Hence, the average shift of the l-th frame is given by

$$\bar{\tau}_i[l] = -T_i \cdot f_s + \left(\frac{N}{2} \bar{\varepsilon}_i[0] + \sum_{\tilde{l}=1}^{l} \bar{\varepsilon}_i \left[\tilde{l} \right] \cdot B \right). \qquad (4)$$

Without loss of generality, the first microphone is selected as reference and the m-th position is regarded in the following. The task at hand can now be described as follows: Estimate the SRO $\bar{\varepsilon}_{12}[l] \approx \bar{\varepsilon}_2[l] - \bar{\varepsilon}_1[l]$ and the STO $\tau_{12}^{\text{STO}} = (T_2 - T_1) \cdot f_s$. Furthermore, we wish to distinguish between the contribution of the STO τ_{12}^{STO} and the TDOF $\tau_{12}^{(m)} = (d_2^{(m)} - d_1^{(m)})/c \cdot f_s$ to the overall signal shift with c denoting the speed of sound and $d_i^{(m)}$ the distance between the i-th microphone and the source at the m-th position.

3. DYNAMIC WEIGHTED AVERAGE COHERENCE DRIFT

In this section, we briefly recapitulate the concept of our previously proposed online weighted average coherence drift (WACD) method

from [6] and describe how it is adapted to the considered dynamic scenario, resulting in the dynamic weighted average coherence drift (DWACD) method.

Online WACD estimates the coherence $\Gamma_{12}^{\tau_{12}^{\text{c}}[\ell]}(\ell B_s, k)$ segment-wisely, where ℓ represents the segment index and B_s the segment shift, and where a segment comprises several frames. Thereby, $\tau_{12}^{\text{c}}[\ell]$ corresponds to an adjustable shift of the segment taken from $y_2[n]$ that coarsely compensates for the SRO-induced signal shift [6]. The coherence is calculated from microphone signal segments of length N_W, where the ℓ-th segment taken from the first microphone starts at $y_1[\ell B_s]$ and the ℓ-th segment taken from the second microphone at $y_2[\ell B_s + \tau_{12}^{\text{c}}[\ell]]$. It is to be mentioned that the SRO is also estimated every B_s samples.

As shown in [4, Eq. (23)] the coherence is given by:

$$\Gamma_{12}^{\tau_{12}^{\text{c}}[\ell]}(\ell B_s, k) \approx H_{12}^{(m)}(k) \cdot W_{\text{SNR}}(\ell, k) \cdot \exp \left(j \frac{2\pi k}{N} \bar{\tau}_{12}^{\text{CD}}[\ell] \right), \quad (5)$$

with $H_{12}^{(m)}(k) = H_1^{(m)}(k) \cdot (H_2^{(m)}(k))^*$ and $W_{\text{SNR}}(\ell, k)$ being a weight depending on the signal-to-noise ratio (SNR) of the time-frequency bins. $\bar{\tau}_{12}^{\text{CD}}[\ell]$ corresponds to the average shift of the ℓ-th segment:

$$\bar{\tau}_{12}^{\text{CD}}[\ell] = -\tau_{12}^{\text{STO}} - \tau_{12}^{\text{c}}[\ell] + \left(\frac{N_W}{2} \bar{\varepsilon}_{12}[0] + \sum_{\tilde{\ell}=1}^{\ell} \bar{\varepsilon}_{12} \left[\tilde{\ell} \right] \cdot B_s \right). \quad (6)$$

The SRO is estimated based on the complex conjugated product of consecutive coherence functions with a temporal distance of $\ell_d B_s$ samples:

$$P_\Gamma(\ell, k) = \Gamma_{12}^{\tau_{12}^{\text{c}}[\ell]}(\ell B_s, k) \cdot \left(\Gamma_{12}^{\tau_{12}^{\text{c}}[\ell]}((\ell - \ell_d) B_s, k) \right)^*. \quad (7)$$

Taking into account that the SRO changes only slowly, the SRO can be approximated by $\bar{\varepsilon}_{12}[\ell]$ in the interval $[(\ell - \ell_d) B_s, \ell B_s]$ resulting in (see [4, Eq. (14)])

$$P_\Gamma(\ell, k) \approx W(\ell, k) \cdot \exp \left(j \frac{2\pi k}{N} \ell_d B_s \bar{\varepsilon}_{12}[\ell] \right), \qquad (8)$$

whereby $W(\ell, k) = \left| H_{12}^{(m)}(k) \right|^2 \cdot W_{\text{SNR}}(\ell, k) \cdot W_{\text{SNR}}^*(\ell - \ell_d, k)$ corresponds to an SNR-related weight.

The DWACD method which is presented in the following utilizes a temporally averaged version of the complex conjugated product of consecutive coherence functions $P_\Gamma(\ell, k)$ to estimate the SRO:

$$P_{\text{WACD}}(\ell, k) = \alpha \cdot P_{\text{WACD}}(\ell - 1, k) + (1 - \alpha) \cdot P_\Gamma(\ell, k), \quad (9)$$

with $P_{\text{WACD}}(-1, k) = 0$ as initial value and α being a smoothing factor close to 1. In contrast to the online WACD method, the DWACD method uses a temporal weighting by the autoregressive smoothing to be able to adapt to fast SRO changes by giving more recent estimates $P_\Gamma(\ell, k)$ a larger weight. Using an energy-based sound activity detection (SAD), the weighted average coherence product is only updated if a source is active in all signal segments needed to calculate $\Gamma_{12}^{\tau_{12}^{\text{c}}[\ell]}(\ell B_s, k)$ and $\Gamma_{12}^{\tau_{12}^{\text{c}}[\ell]}((\ell - \ell_d) B_s, k)$.

A crucial assumption for coherence drift based SRO estimation is that the weight $W(\ell, k)$ does not contribute to the phase of $P_\Gamma(\ell, k)$ [4], which in consequence means that the source position has to be constant during the interval used to compute $P_\Gamma(\ell, k)$. Thus, in a scenario with changing source positions, the DWACD method has to use segments with smaller lengths N_W and smaller time interval ℓ_d between successive coherence functions to avoid or to at least reduce the probability of a speaker change in the estimation interval.

Moreover, the SRO would have to be zero or at least close to zero for the phase of the weight $W(\ell, k)$ to be close to zero [4]. The online WACD method does not specifically address this issue while

the offline WACD method as proposed in [4] utilizes a multi-stage approach with resampling to solve it. The DWACD method takes the SRO estimate of the previous segment $\widehat{\varepsilon}_{12}[\ell-1]$ to resample the segment of $y_2[n]$ which is currently used for coherence estimation. This resampling is realized by a multiplication of the κ-th STFT-frame of the Welch method used for coherence estimation with the phase term $\exp\left(j\frac{2\pi k}{N}\kappa B\widehat{\varepsilon}_{12}[\ell-1]\right)$.

The online WACD method estimates the SRO from the phase of $P_{\text{WACD}}(\ell,k)$, which suffers from the 2π-periodicity of the phase and outlier time-frequency bins, i.e., bins with exceptionally large phase errors. Such outlier time-frequency bins occur more frequently in the multi-position scenario where shorter averaging periods, shorter segments and shorter temporal distances ℓ_d have to be used to calculate $P_{\text{WACD}}(\ell,k)$. Interpreting $P_{\text{WACD}}(\ell,k)$ as a generalized cross power sprectral density (GCPSD) [15] with SNR-based weights, DWACD estimates the SRO using the time lag $\lambda_{\max}$ that maximizes the generalized cross-correlation (GCC) function $p_{\text{WACD}}(\ell,\lambda)$:

$$\widehat{\varepsilon}_{12}[\ell] = -\frac{1}{\ell_d B_s}\cdot\lambda_{\max} = -\frac{1}{\ell_d B_s}\cdot\underset{\lambda}{\operatorname{argmax}}\,|p_{\text{WACD}}(\ell,\lambda)|, \quad (10)$$

with $p_{\text{WACD}}(\ell,\lambda) = \text{IFFT}\{P_{\text{WACD}}(\ell,k)\}$ as the N-point IFFT.

For an accurate SRO estimation a golden section search in the interval $[\lambda_{\max}-0.5, \lambda_{\max}+0.5]$ is used to find the non-integer time lag $\lambda \in \mathbb{R}$ that maximizes $|p_{\text{WACD}}(\ell,\lambda)|$. Note that a settling time is introduced, i.e., the SRO is only estimated for $\ell \geq 40$, to guarantee that $P_{\text{WACD}}(\ell,k)$ from (9) is settled. As discussed in [6], a coarse synchronization of audio streams is necessary for accurate SRO estimation. Consequently, the integer offset between the microphone signals is determined during the first $20\,\text{s}$ of source activity using a cross-correlation, and subsequently compensated before applying DWACD. We propose to use the following parameters: STFT using a Blackman window; $B=2^9$; $N=2^{12}$; $B_s=2^{11}$; $N_W=2^{13}$; $\ell_d = 4$, $\alpha = 0.95$.

4. SAMPLING TIME OFFSET ESTIMATION

In this section a method for STO estimation is proposed that utilizes the SRO compensated signal of $y_2[n]$. The remaining unknown shift between the microphone signals for the m-th source position is given by (see (4) with an additional shift corresponding to the TDOF)

$$\tau_{12} = \tau_{12}^{(m)} - \tau_{12}^{\text{STO}} = \frac{d_2^{(m)} - d_1^{(m)}}{c}\cdot f_s - \tau_{12}^{\text{STO}}. \quad (11)$$

The shift τ_{12} and the distances $d_1^{(m)}$ and $d_2^{(m)}$ needed for STO estimation are segment-wisely estimated with a segment length of 2^{14} samples and a segment shift of 2^{11} samples. The generalized cross-correlation with phase transform (GCC-PhaT) algorithm is used to gather estimates $\hat{\tau}_{12}[\ell]$ for the remaining signal shift. Furthermore, the DNN-based distance estimator [13] with coherent-to-diffuse power ratio (CDR) and STFT as input features is used to estimate the distances $\hat{d}_1^{(m)}[\ell]$ and $\hat{d}_2^{(m)}[\ell]$ of the source to the two sensor nodes.

Based on these estimates, a least squares (LS) problem minimizing the error $\sum_{\ell=0}^{L-1}(\tau_{12}^{\text{STO}}-(\hat{d}_2^{(m)}[\ell]-\hat{d}_\ell^{(m)}[l])/c\cdot f_s+\hat{\tau}_{12}[\ell])^2$ is solved for STO estimation. Hereby, L is the number of considered segments. Segments without source activity are excluded from the LS problem using an energy-based SAD. The LS problem leads to the following STO estimate:

$$\hat{\tau}_{12}^{\text{STO}} = \frac{1}{L}\sum_{\ell=0}^{L}\left(\frac{\hat{d}_2^{(m)}[\ell]-\hat{d}_1^{(m)}[\ell]}{c}\cdot f_s-\hat{\tau}_{12}[\ell]\right). \quad (12)$$

Due to the fact that the shift estimates $\hat{\tau}_{12}[\ell]$ as well as the distance
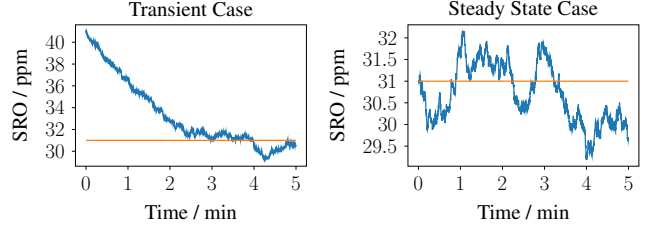
Fig. 1: Example SRO trajectories for a transient case (μ_∞=31ppm; $\epsilon[0]$=μ_∞+10ppm) and steady state case (μ_∞=31ppm; $\epsilon[0]$=μ_∞).

estimates $\hat{d}_1^{(m)}[\ell]$ and $\hat{d}_2^{(m)}[\ell]$ may exhibit large errors (see [16] for an exemplary distribution of the distance estimation error) we embed the LS solver in a random sample consensus (RANSAC) [17] method to remove outliers from the estimation.

5. TIME-VARYING SRO MODEL

In the experiments we model fluctuations of the SRO by an Ornstein-Uhlenbeck process [12]. This process is flexible enough to model both initial transients in SRO, e.g., caused by warm-up after switching on the device, and steady-state fluctuations, e.g., due to changing workload of the processor. The Ornstein-Uhlenbeck process is implemented as an auto-regressive process using the discrete-time Euler-Maruyama approximation:

$$\varepsilon[\ell] = \varepsilon[\ell-1] + \theta\cdot(\mu_\infty - \varepsilon[\ell-1]) + x_\varepsilon[\ell], \quad (13)$$

with smoothing factor $\theta\ll1$, $x_\varepsilon[\ell]\sim\mathcal{N}(0;\sigma_{\text{OU}}^2)$ drawn from a zero-mean Gaussian distribution with variance σ_{OU}^2 and μ_∞ being the mean SRO value reached after all transient effects have died out. In the experiments we set θ=0.001 and $\sigma_{\text{OU}} = 0.05\,\text{ppm}$ resulting in a steady state standard deviation of the SRO of $1.25\,\text{ppm}$ and limit the SRO range for μ_∞ to $\pm100\,\text{ppm}$, which excludes the extreme values reported in [9]. The start value is chosen to be $\varepsilon[0] = \mu_\infty + \Delta_{\text{start}}$ with Δ_{start} in the range $\pm10\,\text{ppm}$. Fig. 1 shows two exemplary SRO trajectories: The left plot displays a transient example simulating a device with a temperature change and the right example showcases a device in a steady state.

Note, if the circuit driving the ADC is using a temperature compensated crystal oscillator (TXCO) the temperature dependent transient effect is marginalized ($\varepsilon[0] := \mu_\infty$) while the other influences remain [18], e.g., the SiT5156 achieves a temperature stability of $\pm0.5\,\text{ppm}$ and has an overall stability of $\pm2.5\,\text{ppm}$.

6. EXPERIMENTS

On a simulated data set, we evaluate the presented STO estimator and the DWACD approach, comparing the latter with two state-of-the-art online SRO estimators[1]. The data is based on the RIR data set (reverberation time T_{60}=300 ms) utilized for geometry calibration in [16]. Using this data set 100 WASNs with four nodes were simulated whereby the first node was used as reference node for SRO and STO estimation. The sensor nodes start recording with an STO in the range $\pm1\,\text{s}$. The nominal sampling frequency is f_s=16 kHz. Each recording is 5 min long and contains a random number of positions M at which up to 4 utterances from the TIMIT data base [19] are used as source signals. Speech pauses with a length between $0.5\,\text{s}$ and $2\,\text{s}$ are optionally added during the source position changes. For the generation of signals with time-varying SROs, which were modeled as described in Sec. 5, the STFT-resampling method from [20] was

---

[1]Source code is available at https://github.com/fgnt/paderwasn

Table 1: Average and maximum RMSE of the SRO estimates and the resulting RMSE of the SRO-induced delay estimates τ_{12}^{ε}

	$\varepsilon \neq$ const.	Multi-Pos.	Silence	Method	avg. RMSE ε_{12} / ppm	avg. RMSE τ_{12}^{ε} / samples	max. RMSE τ_{12}^{ε} / samples
Scenario-1				Online WACD	0.21	0.14	0.50
				DXCP-PhaT	0.15	0.36	0.68
				DXCP-PhaT$_8$	0.69	1.73	3.65
				DWACD	0.40	0.15	0.50
Scenario-2	✓			Online WACD	0.63	0.73	2.09
	✓			DXCP-PhaT	0.66	0.97	2.73
	✓			DXCP-PhaT$_8$	0.95	1.83	4.66
	✓			DWACD	0.51	0.27	1.04
Scenario-3	✓	✓	✓	Online WACD	2.98	6.04	21.00
	✓	✓	✓	DXCP-PhaT	28.96	21.84	161.54
	✓	✓	✓	DXCP-PhaT$_8$	1.31	2.70	7.76
	✓	✓	✓	DWACD	0.57	0.32	1.20
Scenario-4	✓	✓		Online WACD	2.80	3.25	10.96
	✓	✓		DXCP-PhaT	22.42	16.61	160.49
	✓	✓		DXCP-PhaT$_8$	1.28	2.81	6.93
	✓	✓		DWACD	0.64	0.32	1.10

Fig. 2: Influence of the signal length on the STO estimation error for *Scenario-3*

utilized. Sensor noise was added such that the SNR has an average value of $30\,\mathrm{dB}$ for a source-node distance of $3.2\,\mathrm{m}$, which is the average distance on the data set.

In Tab. 1 and Tab. 2 the proposed DWACD method is compared to the online WACD method we presented in [6] and the DXCP-PhaT algorithm [21]. For all algorithms the signals were initially coarsely synchronized as described in Sec. 3 before SRO estimation. The average over the last 160 complex conjugated coherence products is used for SRO estimation in the online WACD method. Due to the fact that the temporal distance between the two signal segments used to calculate the secondary GCPSD function is quite long in the original DXCP-PhaT ($\approx 5\,\mathrm{s}$) and inappropriate for the considered scenario with source position changes, the algorithm is also evaluated with a reduced temporal distance of 8 STFT frames ($\approx 1\,\mathrm{s}$) (denoted as DXCP-PhaT$_8$).

Tab. 1 shows the SRO error for four scenarios with different degrees of dynamicity. Further, the average and maximum error of the SRO-induced delay τ_{12}^{ε}, which is calculated as described in (4), are shown. In *Scenario-1* with constant SRO and a single source position all methods are able to deliver precise SRO estimates. Hereby, the online WACD method and DXCP-PhaT which were designed for such a setup show the best performance. In *Scenario-2* a time-varying SRO is considered. Here, the performance of all estimators degrades, with the DWACD method exhibiting the least degradation.

Taking into account source positions changes (*Scenario-3* and *Scenario-4*) the error grows a lot for the online WACD method and DXCP-PhaT while the error for the DWACD method stays nearly

Table 2: Dependency of the average RMSE / ppm of the SRO estimates on the standard deviation σ_{ε} of $\varepsilon_{12}[\ell]$ for *Scenario-2*

σ_{ε} / ppm	Online WACD	DXCP-PhaT	DWACD
0 - 1	0.55	0.54	0.49
1 - 2	0.60	0.61	0.51
2 - 3	0.63	0.69	0.51
3 - 4	0.71	0.80	0.54
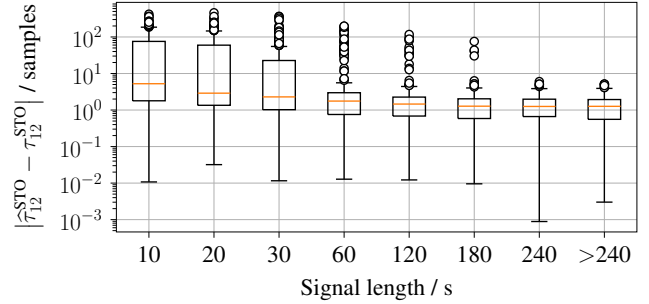
on the same level as for a fixed source position. It is evident, that position changes are more detrimental to the estimation performance than a time-varying SRO. The large errors reported for DXCP-PhaT stem from recordings where in most cases the secondary GCPSD function is calculated from frames corresponding to two different source positions. In contrast to *Scenario-3*, there are no speech pauses in *Scenario-4*, when the speaker position changes. Although DWACD can no longer use the SAD to skip segments during position changes it shows only a small performance degradation.

The dependency of the performance of the different SRO estimators on the standard deviation σ_{ε} of the ground truth SRO process is presented in Tab. 2. For the DWACD method the SRO error is nearly constant despite the growing standard deviation σ_{ε}. In contrast, for the online WACD method and DXCP-PhaT the SRO estimation error is increasing with σ_{ε}.

In Fig. 2 the distribution of the absolute STO error is presented for different signal lengths used for STO estimation. As expected, the STO error gets smaller with growing signal lengths. In most cases, a $1\,\mathrm{min}$ long signal is sufficient to achieve an STO error smaller than $10\,\mathrm{samples}$. However there are some outliers. These outliers disappear for signals which are at least $4\,\mathrm{min}$ long.

7. CONCLUSIONS

In this paper, we present methods for SRO and STO estimation in scenarios with time-varying SROs and source position changes. The former is caused by the time-varying deviation of the sampling frequencies from the nominal sampling frequency, e.g., due to temperature and supply voltage changes, and is modeled as an Ornstein-Uhlenbeck process, while the latter is typical of a meeting scenario with multiple speakers engaged in a communication. It is shown that previously proposed online SRO estimators fail to properly handle the considered dynamic scenario, being particularly vulnerable to source position changes. The presented DWACD algorithm which results from modifying our previously proposed online WACD method handles these aspects by utilizing shorter signal segments for coherence drift estimation in combination with a more robust GCC-based method to estimate the SRO from a temporally weighted average coherence drift. Furthermore, an STO estimation method is presented which uses source-microphone distance estimates to separate the influence of the STO from the TDOFs. Thus, the STO can be removed, while at the same time regarding the geometric arrangement of the WASN.

8. REFERENCES

[1] Shmulik Markovich-Golan, Sharon Gannot, and Israel Cohen, "Blind Sampling Rate Offset Estimation and Compensation in Wireless Acoustic Sensor Networks with Application to Beamforming," in *Proc. International Workshop on Acoustic Echo and Noise Control (IWAENC)*, 2012, pp. 1–4.

[2] Shigeki Miyabe, Nobutaka Ono, and Shoji Makino, "Blind compensation of inter-channel sampling frequency mismatch with maximum likelihood estimation in STFT domain," in *IEEE International Conference on Acoustics, Speech and Signal Processing (ICASSP)*, 2013, pp. 674–678.

[3] Mohamad Hasan Bahari, Alexander Bertrand, and Marc Moonen, "Blind Sampling Rate Offset Estimation for Wireless Acoustic Sensor Networks Through Weighted Least-Squares Coherence Drift Estimation," *IEEE/ACM Transactions on Audio, Speech, and Language Processing*, vol. 25, no. 3, pp. 674–686, 2017.

[4] Joerg Schmalenstroeer, Jahn Heymann, Lukas Drude, Christoph Boeddecker, and Reinhold Haeb-Umbach, "Multi-stage coherence drift based sampling rate synchronization for acoustic beamforming," in *19th International Workshop on Multimedia Signal Processing (MMSP)*, 2017.

[5] Shoko Araki, Nobutaka Ono, Keisuke Kinoshita, and Marc Delcroix, "Estimation of Sampling Frequency Mismatch between Distributed Asynchronous Microphones under Existence of Source Movements with Stationary Time Periods Detection," in *IEEE International Conference on Acoustics, Speech and Signal Processing (ICASSP)*, 2019, pp. 785–789.

[6] Aleksej Chinaev, Gerald Enzner, Tobias Gburrek, and Joerg Schmalenstroeer, "Online Estimation of Sampling Rate Offsets in Wireless Acoustic Sensor Networks with Packet Loss," in *29th European Signal Processing Conference (EUSIPCO)*, 2021, pp. 1–5.

[7] Sharon Gannot, Emmanuel Vincent, Shmulik Markovich-Golan, and Alexey Ozerov, "A consolidated perspective on multi-microphone speech enhancement and source separation," *IEEE/ACM Transactions on Audio, Speech and Language Processing*, vol. 25, no. 4, pp. 692–730, 2017.

[8] Joerg Schmalenstroeer, Patrick Jebramcik, and Reinhold Haeb-Umbach, "A combined hardware-software approach for acoustic sensor network synchronization," *Signal Processing*, vol. 107, pp. 171 – 184, 2015.

[9] "High-precision audio drift measurements with gps," https://protyposis.net/clockdrift/high-precision-audio-drift-measurements-with-gps/, Aug. 2021.

[10] Fred L. Walls and Jean-Jacques Gagnepain, "Environmental sensitivities of quartz oscillators," *IEEE transactions on ultrasonics, ferroelectrics, and frequency control*, vol. 39, pp. 241–249, 1992.

[11] "Sample rate and frequency calibration," https://www.qsl.net/dl4yhf/speclab/frqcalib.htm/soundcard_clock_drift_measurements, Aug. 2021.

[12] George E. Uhlenbeck and Leonard S. Ornstein, "On the theory of the brownian motion," *Phys. Rev.*, vol. 36, pp. 823–841, Sep 1930.

[13] Tobias Gburrek, Joerg Schmalenstroeer, and Reinhold Haeb-Umbach, "On source-microphone distance estimation using convolutional recurrent neural networks," in *Proc. 14th ITG-Symposium Speech Communication*, 2021.

[14] Lin Wang and Simon Doclo, "Correlation Maximization-Based Sampling Rate Offset Estimation for Distributed Microphone Arrays," *IEEE/ACM Transactions on Audio, Speech, and Language Processing*, vol. 24, no. 3, pp. 571–582, 2016.

[15] Charles H. Knapp and G. Clifford Carter, "The generalized correlation method for estimation of time delay," *IEEE Transactions on Acoustics, Speech, and Signal Processing*, vol. 24, no. 4, pp. 320–327, 1976.

[16] Tobias Gburrek, Joerg Schmalenstroeer, and Reinhold Haeb-Umbach, "Geometry calibration in wireless acoustic sensor networks utilizing DOA and distance information," *EURASIP Journal on Audio, Speech, and Music Processing*, vol. 2021, no. 1, pp. 1–17, 2021.

[17] Martin A. Fischler and Robert C. Bolles, "Random sample consensus: A paradigm for model fitting with applications to image analysis and automated cartography," *Commun. ACM*, vol. 24, no. 6, pp. 381395, June 1981.

[18] "TCXO frequency stability and frequency accuracy budget," SiTime, SiT-AN10039 Rev 1.1, Jul. 2014.

[19] John S. Garofolo, Lori F. Lamel, William M. Fisher, Jonathan G. Fiscus, David S. Pallett, Nancy L. Dahlgren, and Victor Zue, "TIMIT acoustic-phonetic continuous speech corpus," 1993, Linguistic Data Consortium (LDC).

[20] Joerg Schmalenstroeer and Reinhold Haeb-Umbach, "Efficient Sampling Rate Offset Compensation - An Overlap-Save Based Approach," in *26th European Signal Processing Conference (EUSIPCO)*, 2018, pp. 499–503.

[21] Aleksej Chinaev, Philipp Thüne, and Gerald Enzner, "Double-Cross-Correlation Processing for Blind Sampling-Rate and Time-Offset Estimation," *IEEE/ACM Transactions on Audio, Speech, and Language Processing*, vol. 29, pp. 1881–1896, 2021.